ACS OMEGA

Open Access

http://pubs.acs.org/journal/acsodf

Article

Application of Carbon Quantum Dots Derived from Waste Tea for the Detection of Pesticides in Tea: A Novel Biosensor Approach

Nitu Sinha and Sonali Ray*

Cite This: *ACS Omega* 2024, 9, 50201−50213

Read Online

ACCESS | Metrics & More | Article Recommendations

ABSTRACT: Chemical pesticide residues have negative consequences for human health and the environment. Prioritizing a detection method that is both reliable and efficient is essential. Our innovative research explored the application of biosensors based on carbon quantum dots (CQDs) derived from waste tea to detect commonly used pesticides in tea. CQDs have been synthesized using a simple one-pot hydrothermal approach and thoroughly characterized using advanced techniques such as high-resolution transmission electron microscopy, ultraviolet−visible spectroscopy, photoluminescence (PL) spectroscopy, Raman spectroscopy, X-ray diffraction, atomic force microscopy, and X-ray photoelectron spectroscopy. The fluorescence resonance energy transfer-based fluorescence "turn on−off" mechanism has been successfully employed to study the detection of four different pesticides, viz., quinalphos 25 EC, thiamethoxam 25 WG, propargite 57 EC, and hexaconazole 5 EC. The detection limits for quinalphos 25 EC, thiamethoxam 25 WG, and propargite 57 EC were determined to be 0.2, 1, and 10 ng/mL, respectively. Notably, these values are significantly lower than the maximum residue level for each pesticide. We achieved a strong linear correlation ($R = -0.96$) with a detection limit of 0.2 ng/mL for quinalphos 25 EC. The quantum yield was determined to be 40.05%. Our research demonstrates that the developed nanobiosensor reliably and accurately detects pesticides, including those present in experimental samples containing mixtures of pesticides.

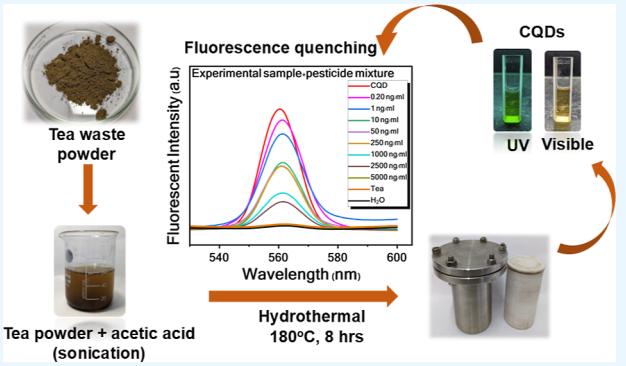

1. INTRODUCTION

Tea, derived from *Camellia sinensis* (L) Kuntze, stands as one of the most extensively consumed nonalcoholic beverages globally, making significant contributions to local economies. However, tea production faces significant challenges from various insect pests, including the tea mosquito bug (*Helopeltis theivora* Wct), tea jassid (*Empoasca flavescens* Fabricius), tea aphid (*Toxoptera aurantii* Boyer), thrips (*Taeniothrips setiventris* Bagn), common looper (*Buzura suppressaria* Guen), red spider mite (*Oligonychus coffeae* Niet), leaf roller (*Gracilaria theivora* Walsm), bunch caterpillar (*Andraca bipunctata* Walk), etc. Addressing these challenges demands a meticulous management approach.[1] Initially, synthetic pesticides and acaricides were employed in tea cultivation to manage the pests. These included organo-synthetic insecticides such as organophosphates, organochlorines, synthetic pyrethroids, and neonicotinoids, along with herbicides and fungicides, which were excessively used in traditional tea gardens to control weeds and pests. Consequently, numerous pesticides were discharged into the environment, posing detrimental effects on both the environment and human health. These effects include the resurgence of major pests, extinction of natural predators, outbreaks of secondary pests, pollution, pesticide resistance, crop damage, decline in honeybee populations, contamination of groundwater, presence of unwanted residues in food items[2] (especially in processed tea), and ultimately, a decline in fish and bird populations.[3] Moreover, even in minimal amounts, pesticide residues have the potential to adversely affect the health of different organisms.

Therefore, regular monitoring is essential to safeguarding consumer health and preventing residue accumulation. Consequently, the challenges underscore the urgent need for a viable method to detect toxicity at a low level and monitor these substances in the environment and food products.[4] Different countries and international bodies have established maximum residue levels (MRLs) for pesticides. Detection of pesticides in food has been accomplished through single and multiresidue analytical methods.[5]

Received: May 10, 2024
Revised: August 20, 2024
Accepted: November 22, 2024
Published: December 9, 2024

Currently, laboratories utilize various methods to detect pesticides, such as high-performance liquid chromatography (HPLC),[6] liquid chromatography−tandem mass spectrometry (LC-MS/MS),[7] capillary electrophoresis (CE), gas chromatography, and mass spectrometry.[8] HPLC is distinguished by its high resolution, rapid analysis, and sensitivity with minimal sample requirement.[9] Both gas and liquid chromatography techniques offer high sensitivity and selectivity. Similarly, electrochemical sensors (including amperometry, conductometry, voltammetry, and potentiometry) provide real-time monitoring with moderate sensitivity and carbon footprint.[10] CE delivers highly sensitive and swift high-resolution separation using diverse detection methods.[11] However, these techniques have limitations; for instance, HPLC necessitates significant solvent quantities.[12] Other chromatographic methods require multistep sample preparation, which is labor-intensive and time-consuming. Moreover, these instruments are costly and have a substantial carbon footprint,[10] making them impractical as readily available sensors due to calibration complexities.

Recently, various nanobiosensors have emerged alongside traditional chromatographic methods for pesticide testing. These biosensors include an electrochemical biosensor utilizing a polyimide substrate coated with MnO_2 nanosheets and a laser-induced graphene electrode[13] for pesticide detection. Additional approaches involve specific detection of the organophosphate insecticide paraoxon using CeO_2@NC enzymes[14] and nitrogen-enriched conjugated polymer-assisted metal-free carbon enzymes.[15] Similarly, glyphosate detection employs a phosphatase-like enzyme[16] and a cobalt-doped Ti_3C_2MXene enzyme-mediated electrochemical strategy,[17] marking significant advancements in pesticide detection research.

Fluorescence-enhancing and quenching mechanisms are commonly employed for detecting pesticides, particularly for organophosphates and neonicotinoids.[18−20] Previous studies have identified gold,[21−23] silver,[18] graphene,[19,20] and aptasensor[24] nanoparticles as nanoquenchers in pesticide detection. A diverse array of fluorescent-based sensors have been developed, incorporating organic dyes, luminescent proteins, metal−organic frameworks, and quantum dots. Notably, zero-dimensional materials such as carbon quantum dots (CQDs), including carbon nanoparticles (CNPs), are highly acknowledged due to their exceptional photostability, biocompatibility, chemical stability, cost-effectiveness, straightforward synthesis, intense fluorescence, large surface area, versatile functionalization, and minimal toxicity.[25] CNPs generally show a semispherical morphology with an amorphous to nanocrystalline structure, mainly made up of oxygen−nitrogen-based groups. They also possess post-modified functional groups facilitating easy interaction and binding to target molecules.[26] CQDs, often derived from natural sources or nontoxic precursors, offer cost-effective solutions suitable for large-scale biosensing applications.[27] The versatility and efficacy of CQDs underscore their pivotal role in advancing pesticide detection technologies.

CQDs can be manufactured through various methods, including hydrothermal synthesis,[28] electrochemical synthesis,[29] and microwave-assisted synthesis.[30] Among these techniques, hydrothermal synthesis stands out for its ability to yield high-quality materials with excellent dispersion and straightforward control over particle size, facilitated by the even distribution of ions in the aqueous solution.[31−35] Recent research has highlighted the remarkable efficacy of CQDs in evaluating food quality and safety.[36] Investigations have explored dual-mode visual and smart sensing applications using a glyphosate nanosensor based on carbon dots. This sensor boasts a critical detection limit of 0.8 ng/mL and a high quantum yield.[37] Fluorescence biosensors play a pivotal role in environmental monitoring, leveraging their capabilities for fluorescence quenching and enhancement. Accurate pesticide detection has been achieved through a fluorescence resonance energy transfer (FRET)-based sensing mechanism. Additionally, studies have explored pesticide detection techniques employing the inner filter effect, which operates at distances exceeding 20 nm, in contrast to FRET, which occurs within a range of less than 10 nm. Both techniques demonstrate superior selectivity and sensitivity compared to enzyme catalysis.[38−40]

Numerous recent studies have focused on synthesizing CQDs from natural sources.[41,42] However, the synthesis of CQDs from tea waste remains sporadic.[43] To the best of our knowledge, no existing research explores the potential of utilizing tea waste for pesticide detection in tea. This novel approach not only tackles the issue of waste disposal but also offers a dependable and cost-effective method for pesticide detection in tea.

Therefore, to address these critical challenges, we developed an advanced fluorescent nanosensor using CQDs derived from unused tea leaf waste after the tea infusion process. The synthesis method involved an ecofriendly hydrothermal process that utilized residual tea waste as a carbon source, resulting in water-soluble green fluorescent tea-CQDs. It had a higher quantum yield than other natural carbon source-derived CQDs. To our knowledge, our study is the first to demonstrate the detection of commonly used tea pesticides (propargite 57 EC, thiamethoxam 25 WG, hexaconazole 5 EC, and quinalphos 25 EC) using tea-derived nanosensors (CQDs) based on a fluorescence "turn on−off" mechanism. Our nanosensors exhibit detection limits significantly lower than MRL values. We analyzed pesticide concentrations and their correlations with fluorescence intensity. These nanosensors are cost-effective, highly selective, and sensitive, making them ideal for the detection of environmental pollutants. Additionally, we validated their accuracy using tea infusion as an experimental sample. By highlighting the potential of waste tea utilization, our research underscores the importance of sustainable practices in the tea industry, making substantial contributions to environmental conservation and public health.

2. EXPERIMENTAL SECTION

2.1. Reagents and Instruments. The sample used for CQDs preparation was tea leaf waste obtained after tea infusion preparation, serving as a carbon source. Throughout the synthesis process, HPLC-grade water was utilized. Acetic acid (Sigma-Aldrich), a 0.22 μm membrane filter, Whatman no-1 filter paper, analytical-grade quinine sulfate, phosphate buffer solution (PBS), and Tea Board of India-approved pesticides for Indian tea gardens (including thiamethoxam 25 WG, propargite 57 EC, hexaconazole 5 EC, and quinalphos 25 EC) were employed for the detection of analysis.

UV light with a wavelength of 365 nm facilitated the observation of the CQDs solution's color. Fluorescence and ultraviolet−visible (UV−vis) spectroscopy techniques were utilized to determine the luminescence characteristics of the CQDs. High-resolution transmission electron microscopy

https://doi.org/10.1021/acsomega.4c04449
ACS Omega 2024, 9, 50201−50213

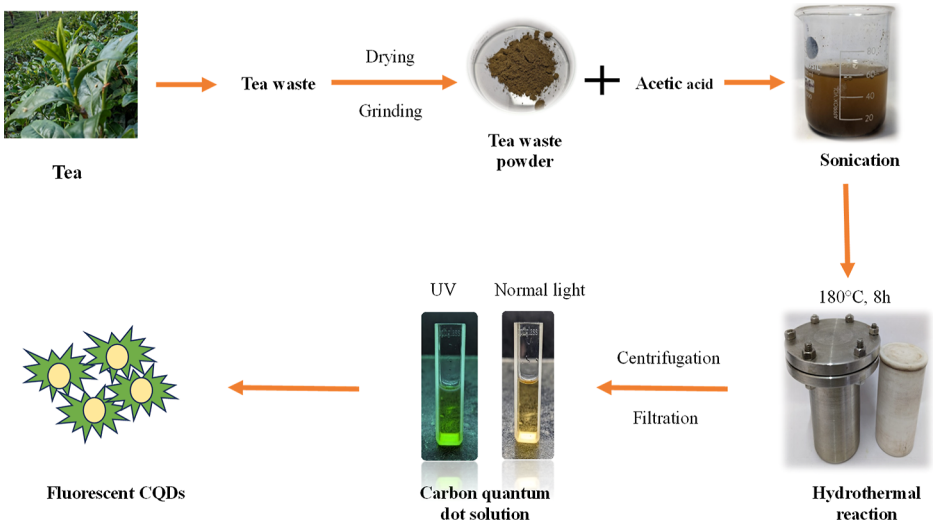

Figure 1. Synthesis of CQDs from tea waste.

(HRTEM) aided in characterizing the morphology and determining sample size. Raman spectroscopy provided insights into the chemical structure, crystallinity, and molecular interactions. X-ray diffraction (XRD) was employed to analyze crystallinity, while atomic force microscopy (AFM) was used to investigate the surface topography and size range of the CQDs. X-ray photoelectron spectroscopy (XPS) analysis was conducted to investigate the elemental composition of the CQDs.

2.2. Synthesis of CQDs. CQDs were derived from accumulated unused tea leaf waste following the preparation of tea infusion by employing an environmentally friendly hydrothermal method (Figure 1). Initially, 0.2 g of tea waste powder was combined with 60 mL of a 20% acetic acid solution in a 100 mL beaker. Subsequently, the mixture underwent sonication for 30 min. This prepared mixture was transferred into a Teflon-coated reactor and subjected to a reaction at 180 °C for 8 h in a hot air oven. Afterward, the solution was allowed to cool to room temperature. The resulting yellow to light brown solution underwent centrifugation at 12,000 rpm for 15 min, followed by filtration through a 0.22 μm membrane filter twice to obtain a yellow-colored CQDs solution, which was then stored at 4 °C for further analysis.

2.3. Characterization of CQDs. *2.3.1. UV−Vis Spectroscopy.* In our investigation, 1 mL of crude CQDs solution, obtained via hydrothermal methods, was diluted 1000-fold using HPLC-grade water and subjected to sonication before analysis under a UV−vis spectrometer (Systronics). The instrument features a high-resolution, dependable, single-beam setup with digital wavelength adjustment (in 0.1 nm increments), a 0.5 nm bandwidth, and a flexible range facilitated by a low-noise photo multiplier tube detector. The spectral recording was conducted within the range 200−1000 nm. HPLC-grade water served as the medium for the blank and reference measurements.

2.3.2. High-Resolution Transmission Electron Microscopy. The structural characteristics, including shape, size, and spatial arrangements of the CQDs, were examined by using HRTEM. Initially, the sample solution was subjected to ultrasonication, and droplets were then deposited onto TEM grids. Subsequently, the drop-casted samples on TEM grids were left to air-dry at room temperature for 12 h. Carbon films (50 nm) were applied and exposed to infrared radiation for 2 min. All TEM images were captured using a Technai HRTEM instrument that operated at an accelerating voltage of 200 kV and was equipped with a camera.

2.3.3. Raman Spectroscopy. Raman spectra were captured by using the EnSpectr instrument. This device utilizes a 30 mW single mode 532 nm laser, a 20 (30 optional) μm entry slit, an 1800 g/mm holographic grating, a state-of-the-art low-pass filter, and other advanced components, enabling precise Raman and luminescent measurements across a wide spectrum range from 100 to 4000 cm^{-1}. The integration time for measurements was set at 10 s. The experiments were conducted at room temperature utilizing a 100× objective, with the laser power maintained below 1.2 mW to prevent sample degradation.

2.3.4. Photoluminescence Spectroscopy. Photoluminescence excitation (PLE) spectra were obtained using the PTI (Photon Technology International) Quanta Master TM 300 phosphorescence/fluorescence spectrofluorometer equipped with a pulsed xenon source for excitation. The spectroscope's detection system comprised a photon-counting detector and a monochromator featuring a single grating. Felix GX software facilitated all of the data collection processes. Excitation occurred within the range of 280 nm, while emission was measured within the 300−600 nm range. A slit size of 1.25 mm and an integration time of 0.5 s were employed for each measurement.

2.3.5. XRD Pattern. XRD analysis of the CQDs was conducted by using a Bruker D8 Discoverer X-ray diffractometer. The instrument performed a 2θ scan at 20 mA and 40 kV. Employing Ni-filtered Cu Kα radiation (λ = 1.54056 Å) in reflection geometry, the diffractometer was equipped with a position-sensitive detector. The XRD analysis utilized a slow scanning speed and a small step size for 2θ values ranging between 10 and 70°.

2.3.6. Atomic Force Microscopy. The NTEGRA SPECTRA-NT-MDT spectrum instruments were employed to capture the topographical image of the synthesized CQDs in a noncontact mode, with analysis conducted using Gwyddion software.

https://doi.org/10.1021/acsomega.4c04449
ACS Omega 2024, 9, 50201−50213

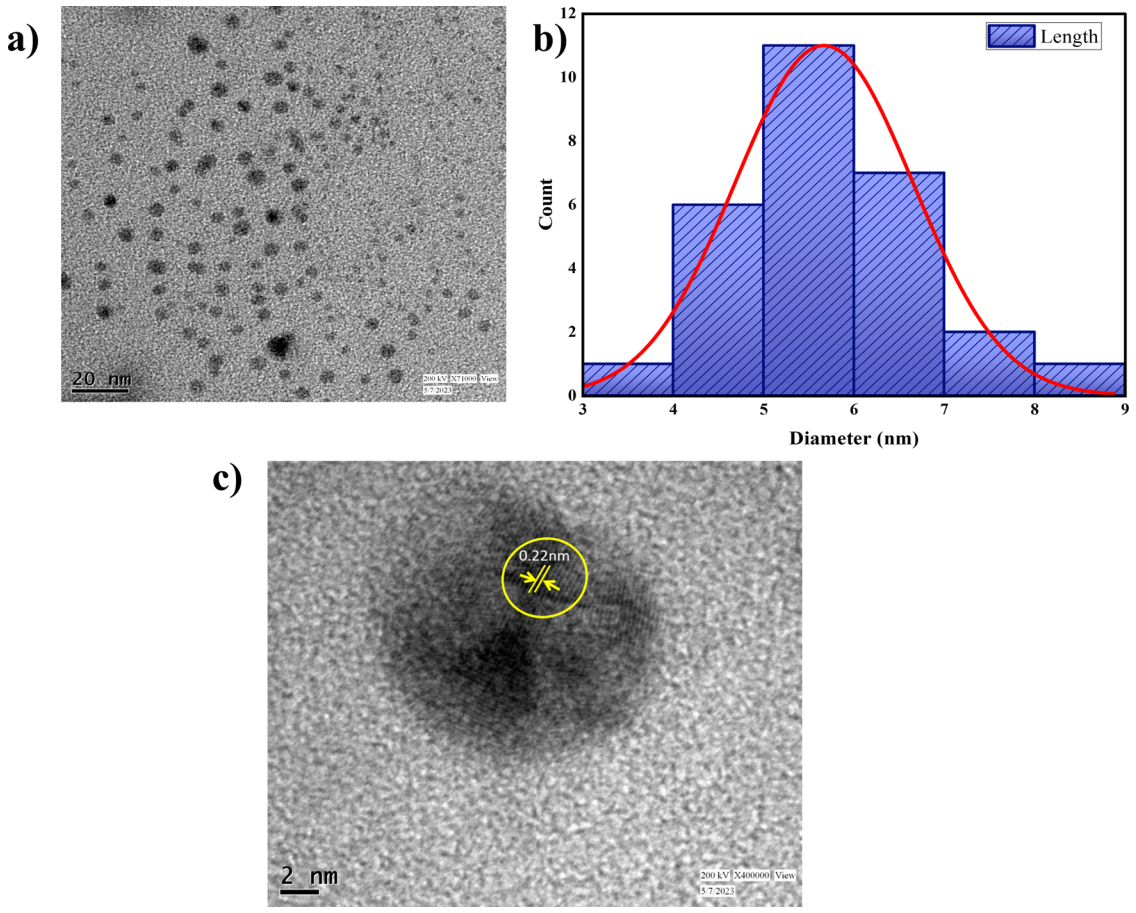

Figure 2. Characterization of CQDs: (a) HRTEM image depicting CQDs, (b) histogram illustrating the size distribution of CQDs, and (c) HRTEM image revealing clear lattice spacing with an interfringe distance of 0.22 nm.

2.3.7. X-ray Photoelectron Spectroscopy. In our study, the hydrothermally derived filtrate containing CQDs was freeze-dried to identify the chemical constituents. XPS analysis was performed using a Thermo Fisher K-Alpha photoelectron spectrometer equipped with a 180° double-focusing hemispherical analyzer, a 128-channel detector, a monochromatic X-ray source, and an ion gun capable of an energy range from 100 to 4000 eV.

2.4. Quantum Yield. The fluorescence quantum yield (Q) represents the ratio of absorbed to emitted photons, reflecting the efficiency of the fluorescence emission. Quinine sulfate (φ = 0.54 in 0.05 M H_2SO_4) served as the reference sample. Both the reference sample and the synthesized CQDs exhibited a refractive index of approximately 1.33. The following equation is utilized for the quantum yield calculation.

$$Q_x = Q_r \times \frac{A_r \times I_x \times \eta_x^2}{A_x \times I_r \times \eta_r^2} \quad (1)$$

In the provided equation, "Q" denotes the quantum yield, "A" represents the absorbance at the excitation wavelength, "I" signifies the emission value at the stimulating wavelength, and "η" denotes the refractive index value. Additionally, the subscripts "x" and "r" pertain to the CQDs and reference sample, respectively. This quantum yield calculation method offers several advantages over traditional optical approaches, including enhanced accuracy, user-friendly operation, minimal sample consumption, and wide-ranging applicability.[39] Previous research has suggested that a high quantum yield may enhance selectivity and narrow the detection limit range for sensors based on CQDs.[3]

2.5. Detection of Pesticides Using CQDs. The synthesized CQDs serve as a tool for pesticide detection.[40] In this study, quinalphos 25 EC, thiamethoxam 25 WG, propargite 57 EC, and hexaconazole 5 EC were selected as model pesticides to evaluate the effectiveness of CQDs as biosensors. Positive controls consisted of CQDs solution with maximum fluorescence emission, while negative controls utilized HPLC-grade water.

Various concentrations of the pesticides as mentioned above (0.2, 1, 10, 50, 250, 1000, 2500, and 5000 ng/mL) were combined with CQDs solutions. The fluorescence intensity of CQDs was then measured in the presence of each pesticide to assess their individual fluorescence quenching or enhancing efficacy. Additionally, all four pesticides were combined in the same sample at different concentrations, and their collective quenching or enhancing ability was evaluated due to their dynamic interactions.

The hydrothermally derived CQDs solution was initially diluted 1000 times with HPLC-grade water. Subsequently, 800 μL of CQDs mixed with 400 μL of PBS (pH = 7.4) was pipetted into a 3 mL vial. Next, 800 μL of each pesticide solution (at concentrations of 0.2, 1, 10, 50, 250, 1000, 2500, and 5000 ng/mL) was added separately and in combination.

To ensure optimal conditions, the reaction mixtures were incubated for 30 min at 37 °C, after which the fluorescence intensity was measured using a photoluminescent spectropho-

https://doi.org/10.1021/acsomega.4c04449
ACS Omega 2024, 9, 50201−50213

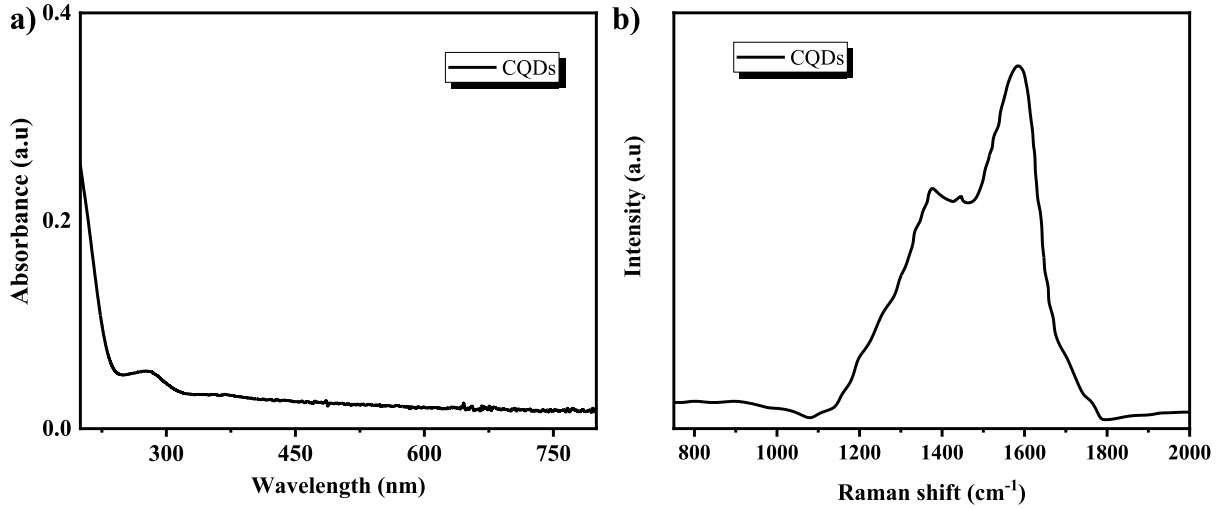

Figure 3. (a) UV−vis spectroscopy analysis of CQDs. (b) Raman spectrum of CQDs.

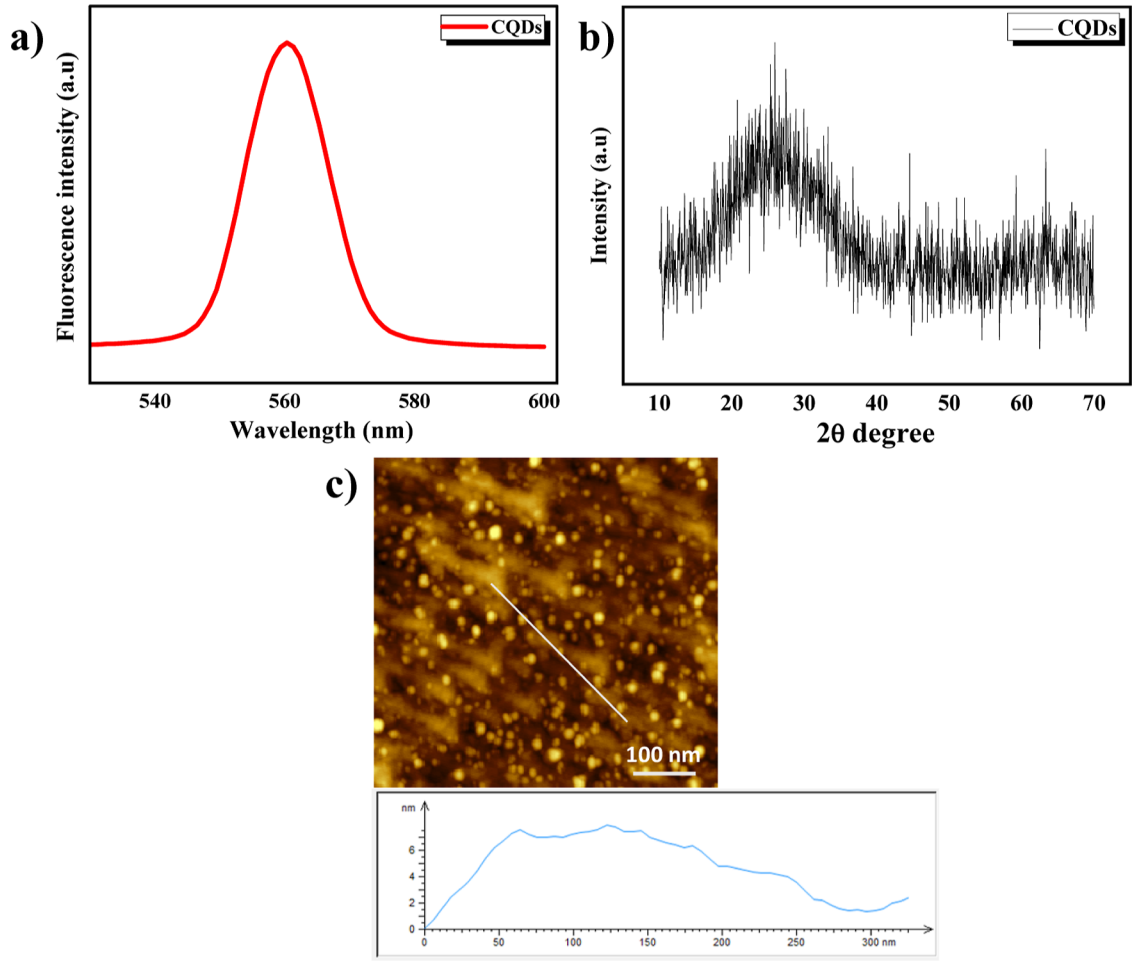

Figure 4. (a) PL intensity of fluorescent CQDs, (b) XRD pattern of CQDs, and (c) AFM image depicting CQDs and their size distribution.

tometer. HPLC-grade water served as the negative control, while the CQDs solution acted as the positive control for the experiment.

2.6. Detection of Pesticides (Quinalphos 25 EC, Thiamethoxam 25 WG, Propargite 57 EC, and Hexaconazole 5 EC) in Tea Infusions (Experimental Sample) Using CQDs. The CQDs-based method was employed to detect tea adulteration with specific pesticides (quinalphos 25 EC, thiamethoxam 25 WG, propargite 57 EC, and hexaconazole 5 EC) to evaluate its practical utility. Pesticide-free Darjeeling orthodox black tea from the second flush was selected as the experimental sample (standard) to assess the detection potential of the CQDs.

https://doi.org/10.1021/acsomega.4c04449
ACS Omega 2024, 9, 50201−50213

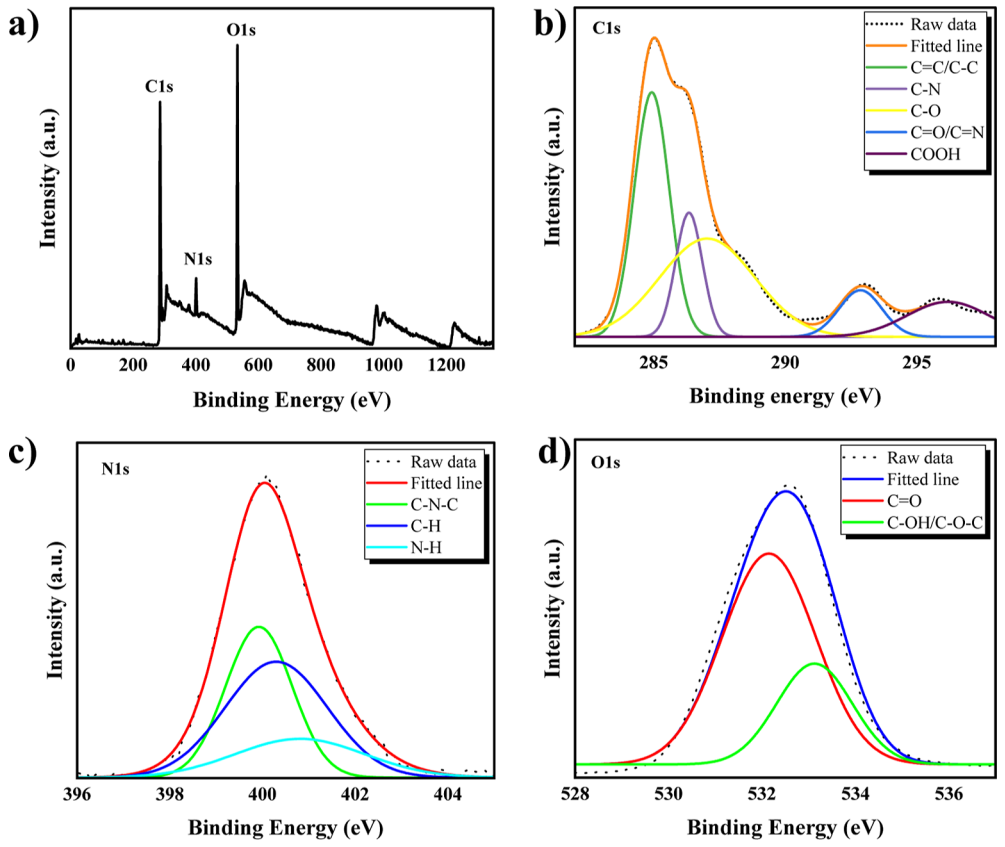

Figure 5. XPS spectra of CQDs derived from tea waste. (a) XPS survey spectrum. High-resolution spectra of (b) C 1s, (c) N 1s, and (d) O 1s.

Each adulterated tea sample was prepared as 2 g of pesticide-free standard tea sample was boiled with 20 mL of HPLC-grade water for 5 min. After cooling at room temperature, the mixture was filtered, and the resulting tea infusion was transferred to a beaker and sonicated for 5 min to ensure uniform dispersion. The tea infusion was then diluted 10 times with PBS buffer (pH 7.4). Subsequently, 1 mL of tea infusion was combined with 1 mL of various pesticide concentrations (0.2, 1, 10, 50, 250, 1000, 2500, and 5000 ng/mL). Each solution mixture was vortexed for 2 min and filtered.

The experimental adulterated tea samples were detected using the same technique as outlined in Section 2.5. A solution containing only CQDs with pesticide-free tea infusion served as the positive reference, while the tea infusion alone served as the negative reference.

To prepare the reaction mixture, 800 μL of CQDs (diluted 1000 times) with 400 μL of PBS (pH 7.4) was pipetted into a 3 mL vial. Next, 800 μL of each experimental sample (containing pesticides) was added separately. The reaction mixtures were then incubated for 30 min at 37 °C. Finally, the fluctuations in the fluorescence intensity of CQDs in the experimental sample were assessed using a photoluminescent spectrophotometer.

3. RESULTS AND DISCUSSION

3.1. CQDs Characterization and Determination of Quantum Yield. Figure 2a presents the HRTEM image of CQDs, revealing densely packed nanoparticles with irregular spherical shapes ranging from 3 to 9 nm. The average size distribution, depicted in the histogram shown in Figure 2b, was 5−6 nm. Figure 2c illustrates lattice fringes of CQDs with clear lattice spacing, indicating an interfringe distance of 0.22 nm, corresponding to the (002) facet of graphene's sp^2 graphitic crystal phase.[44]

The absorption and emission properties of the CQDs were analyzed according to their optical characteristics. As depicted in the UV−vis spectra (absorption features) shown in Figure 3a, all CQDs demonstrated broad absorption across the UV region, with spectral tails extending into the near-visible region. At 280 nm, each CQD sample displayed an absorption behavior.

In Figure 3b, the Raman spectra of CQDs are illustrated. Two characteristic bands, D (associated with sp^3-hybridization) and G (related to sp^2-hybridization), were observed at 1373 cm^{-1} and 1585 cm^{-1}, respectively. The G band arises from the E_{2g} mode in the two-dimensional hexagonal graphite lattice, representing the vibrations of sp^2-bonded carbon atoms. Conversely, the D band is indicative of structural disorder within the graphite sp^2 cluster, attributed to vibrations of dangling bonds in the termination plane.[45]

The PL spectra exhibit a peak at 561.36 nm, as illustrated in Figure 4a. Figure 4b displays the XRD pattern of CQDs, specifically depicting the (002) plane. Due to the relatively small size of the obtained CQDs, a broad diffraction peak emerged, centered at approximately 22.0°. This peak corresponds to the lattice spacing of carbon materials along the (002) plane.[45]

To validate the size distribution, we conducted additional AFM of the quantum dots, which revealed a size distribution consistent with HRTEM images, as depicted in Figure 4c. The AFM image confirmed that the carbon dots are within the range of 10 nm. It provided a topographical representation of the produced CQDs.

https://doi.org/10.1021/acsomega.4c04449
ACS Omega 2024, 9, 50201−50213

The elemental composition and oxidation states of the produced CQDs samples were confirmed through XPS analysis, as depicted in Figure 5a. The XPS spectra illustrate three elements: C 1s at 286.18 eV, N 1s at 400.98 eV, and O 1s at 532.98 eV, with atomic percentages of C-65.55%, N-5.81%, and O-28.64%, respectively. A detailed examination of the C 1s high-resolution deconvoluted spectra (Figure 5b) reveals five distinct peaks at 284.87, 286.30, 287.1, 292.90, and 296.23 eV corresponding to C═C/C−C of graphitic carbon, C−N, C−O, C═O/C═N bonds, and COOH group, respectively. The N 1s deconvoluted spectra exhibit peaks at 399.92, 400.34, and 401.1 eV attributed to C−N−C, C−N, and N−H (amino) bonds, respectively (Figure 5c),[46,47] indicating the presence of electron-rich amino groups on the CQDs surface. Additionally, the O 1s spectra display distinct peaks at 532.14 and 533.2 eV (Figure 5d), corresponding to C═O and C−OH/C−O−C bonds, respectively. These findings demonstrate the functionalization of CQDs with carbonyl, carboxyl, hydroxyl, and amino groups, enhancing their water solubility without additional chemical modifications, thereby making them suitable for sensor applications.[48]

Quantum yield was determined using eq 1, resulting in a fluorescence quantum yield of 40.05% at an excitation wavelength of 280 nm. Quinine sulfate served as a reference sample for comparison. Our investigation revealed that the quantum yield of CQDs derived from tea waste is significantly higher than that of other natural precursors, as summarized in Table 1.

Table 1. Comparison of the Quantum Yield (Q) of CQDs Prepared by Numerous Natural Precursors

sl no.	source	size (nm)	color	Q (%)	refs
1	*Punica granatum* fruit	3.5	blue	7.6	49
2	apple juice	4.5 ± 1.0	blue	4.27	50
3	willow bark	1−4	blue	6	51
4	apple juice	2.8 ± 0.4	blue	6.4	52
5	mushroom (fungus)	2.3	blue	15.3	53
6	strawberry juice	5.2	blue	6.3	54
7	carrot juice	5.5	blue	5.16	55
8	orange juice	2.5	green	26	56
9	tea waste	5−6	green	40.05	our study

3.2. Detection of Specific Pesticides (Individually and in Combination) and Exploring Their Impact on Fluorescence through a "Turn On−Off" Mechanism.

Our hypothesis suggests that introducing chemical pesticides alongside CQDs induces collisional activation or deactivation of excitation intensity, influenced by different binding affinities, ultimately serving as an intensity-enhancing or quenching agent. Accordingly, we devised an assay utilizing CQDs as fluorescent signal sources to track different pesticide concentrations.

Fluorescence quenching and enhancement were observed across concentrations of 0.2, 1, 10, 50, 250, 1000, 2500, and 5000 ng/mL during the interaction between selected pesticides and CQDs. The four chosen pesticides were detected individually and in combination. Notably, concentration-dependent quenching and fluorescence increments were detected under a UV lamp.

3.2.1. Individual Detection of Four Pesticides Using CQDs. Propargite 57 EC was undetectable at concentrations of 0.2 and 1 ng/mL. However, it was readily detectable at a concentration of 10 ng/mL, as illustrated in Figure 6a. A detection limit of 10 ng/mL was determined, showcasing an exceptionally high quenching ability at 5000 ng/mL. In contrast to other pesticides, propargite 57 EC exhibited nearly identical quenching ability to water (used as a negative control) at a 5000 ng/mL concentration. The study also observed changes in fluorescence color under UV light (365 nm) with increasing pesticide concentrations. Figure 6a shows a notable decrease in fluorescence emission peaks as pesticide concentrations ranged from 0.2 to 5000 ng/mL.

Conversely, Figure 6b illustrates that the addition of various concentrations of pesticide (thiamethoxam 25 WG) significantly reduces the fluorescence intensity in a concentration-dependent manner. Unlike quinalphos 25 EC, thiamethoxam 25 WG did not exhibit significant changes in the fluorescent intensity at 0.2 ng/mL, as depicted in Figure 6b. However, the detection limit for thiamethoxam 25 WG showed slight variation. At 1 ng/mL, thiamethoxam 25 WG exhibited a decrease in fluorescent intensity compared to the previous concentration; this quenching trend of fluorescence intensity persisted with subsequent increasing concentrations.

The fluorescence intensity quenching was observed with thiamethoxam 25 WG and propargite 57 EC. It is likely that in an aqueous solution of pesticides, the functional groups of CQDs undergo conversions such as COOH to COO^- and H^+, OH to O^- and H^+, and NH_3 to $-NH_3^+/-NH$, respectively. Within an aqueous environment, CQDs may form complexes through ionic interactions and hydrogen bonding, leading to the stacking of CQDs. This eventually diminishes their fluorescence intensity through energy transfer from CQDs to pesticides via the FRET mechanism, resulting in CQDs quenching.

Subsequently, Figure 6c illustrates that the quenching effect of hexaconazole 5 EC is negligible compared with that of other pesticides. Moreover, a concentration-dependent quenching trend is absent in hexaconazole 5 EC compared to other pesticides (propargite 57 EC and thiamethoxam 25 WG). This specific phenomenon can be attributed to the component specificity of CQDs. Not every pesticide is capable of interacting with, quenching, or enhancing the fluorescence intensity of CQDs. This distinctiveness elucidates the specificity of CQDs in distinguishing between thiamethoxam 25 WG, propargite 57 EC, and quinalphos 25 EC from hexaconazole 5 EC.

In Figure 6d, it can be observed that the fluorescence intensity of CQDs noticeably escalates with the increasing concentration of pesticide quinalphos 25 EC ranging from 0.2 to 5000 ng/mL. Even at the lowest concentration of 0.2 ng/mL, quinalphos 25 EC demonstrates a discernible impact on fluorescence intensity, with its peak steadily rising to confirm the presence of the pesticide. This fluorescence intensity continues to trend upward as the pesticide concentration increases significantly. Furthermore, under UV light, alterations in the solution's color, transitioning from green to a vivid green hue, were noted with escalating concentrations of quinalphos 25 EC.

In this scenario, the surface of CQDs derived from tea waste contains carboxyl, hydroxyl, and amine groups. These functional groups enable CQDs to potentially bind with the highly reactive phosphorothioate group of the quinalphos 25 EC pesticide through their amino groups. Meanwhile, carboxyl and hydroxyl groups may remain unbound on the surface,

https://doi.org/10.1021/acsomega.4c04449
ACS Omega 2024, 9, 50201−50213

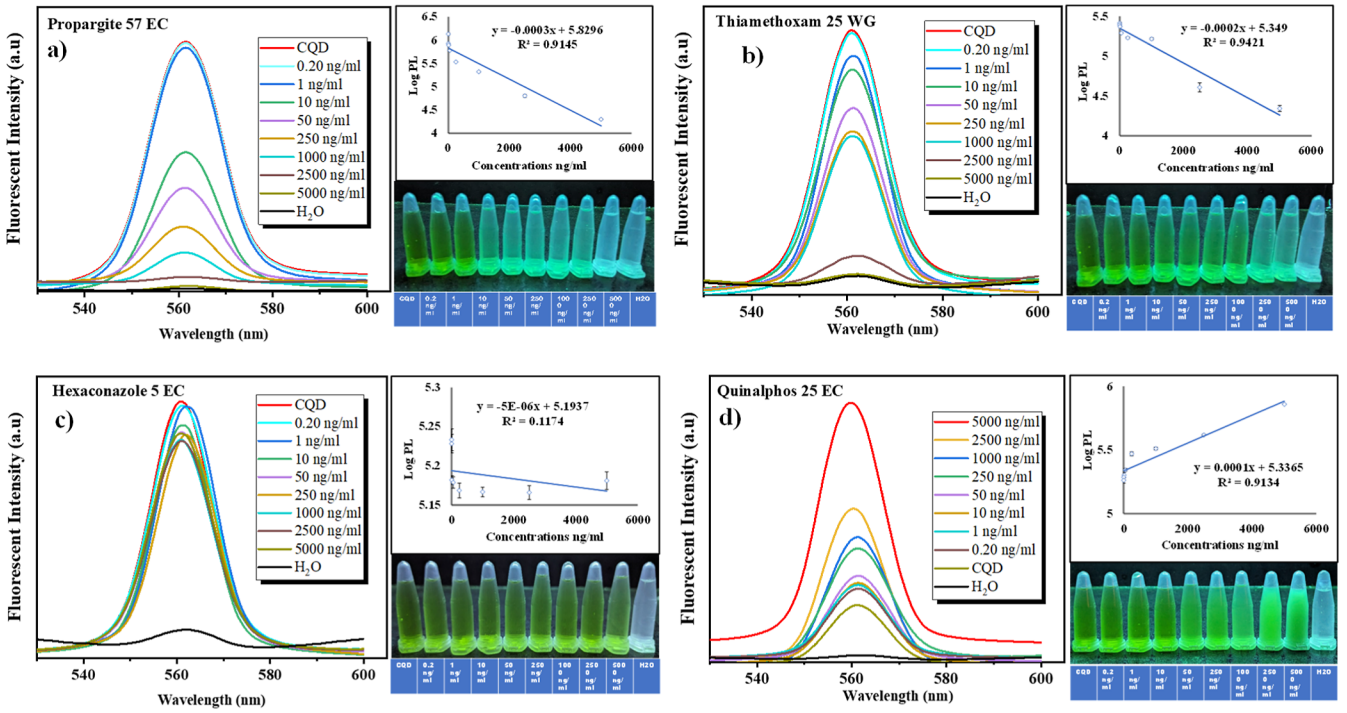

Figure 6. Various concentrations (0.2, 1, 10, 50, 250, 1000, 2500, and 5000 ng/mL) of different pesticides, namely, (a) propargite 57 EC, (b) thiamethoxam 25 WG, (c) hexaconazole 5 EC, and (d) quinalphos 25 EC, were introduced to CQDs samples. Changes in fluorescence intensity were observed under PL and UV light conditions, and a concentration-dependent graph is presented using logarithmic values.

Table 2. Analytical Characteristics of Various Common Sensing Techniques Utilized for Determining the Levels of Thiamethoxam 25 WG, Quinalphos 25 EC, Propargite 57 EC, and Hexaconazole 5 EC

sl no	pesticides	utilized in	analytical method	detection limit	refs
1	thiamethoxam 25 WG		RP-HPLC	0.119 μg/mL	57
		food sample	electrochemical	4.9 nM	58
			GO-SELEX	0.37 nM	59
2	quinalphos 25 EC	vegetable	chemiluminescence assay	0.0055 μg/mL	60
3	propargite 57 EC	black tea	HPLC	5.07 mg/kg	61
4	hexaconazole 5 EC	surface water	LC−MS/MS	0.07 mg/L	62

weakening their self-complexation and resulting in isolated or detached CQDs. Consequently, their fluorescence intensity increases compared to that when they are not detached. This phenomenon could facilitate the development of a CQDs-based "turn-on" sensor for this insecticide, with fluorescence enhancement occurring through the FRET mechanism.

A linear curve was utilized to graph the logarithm of fluorescence emission from CQDs against the pesticide concentrations (C) to assess quenching levels in the peak sensitivity analysis. Excel-2021 was employed to analyze the correlation between pesticide concentrations and logarithmic fluorescence intensities, revealing a robust correlation between the concentration of thiamethoxam 25 WG, quinalphos 25 EC, and propargite 57 EC and their respective logarithmic fluorescence intensities. Specifically, thiamethoxam 25 WG and propargite 57 EC exhibited negative correlation values of −0.97 and −0.96, respectively, indicating that fluorescence intensity decreases as the pesticide concentration increases. Conversely, quinalphos 25 EC displayed a positive correlation value of 0.96, suggesting that the fluorescence intensity increases with increasing pesticide concentration. In contrast, hexaconazole 5 EC exhibited a weak correlation, with a value of −0.34. These findings elucidate the relationship between the pesticide concentration and fluorescence intensity.

This study has achieved the lowest detection limit compared to alternative pesticide recognition methods that utilize the fluorescence characteristics of CQD materials. The approach exhibits remarkable sensitivity and offers a broad detection range. Previous studies on nanoparticles have reported detection limits of 2 ng/mL for quinalphos and 16 ng/mL[50,51] for thiamethoxam 25 WG, with no prior reports on the detection of propargite 57 EC and hexaconazole 5 EC using CQDs. Hence, it can be inferred that CQDs synthesized via green synthesis possess a greater biocompatibility potential than those produced using conventional precursors.

The synthesized CQDs' selectivity is demonstrated by their lack of fluorescence quenching upon interaction with hexaconazole 5 EC. The estimated detection limits for quinalphos 25 EC, thiamethoxam 25 WG, and propargite 57 EC are 0.2, 1, and 10 ng/mL, respectively. Additionally, Table 2 provides insights into the analytical performance of the proposed method across various commonly utilized sensing modalities for the listed pesticides.

This study has been found to possess a significantly lower detection limit compared to the MRL of the selected pesticides

https://doi.org/10.1021/acsomega.4c04449
ACS Omega 2024, 9, 50201−50213

examined in this study, as detailed in Table 3, which highlights their use in tea gardens.

Table 3. Four Chosen Pesticides, along with Their MRL Values and the Detection Limits (in ppm) Determined in Our Study

sl no	type of pesticide	name of the pesticide	MRL value (ppm)	detection limit with CQDs (ppm)
1	neonicotinoid	thiamethoxam 25 WG	20	0.001
2	acaricide	propargite 57 EC	10	0.01
3	fungicide	hexaconazole 5 EC	5	NA
4	organophosphate	quinalphos 25 EC	0.7	0.0002

3.2.2. Pesticide Mixture. The four selected pesticides were combined as a pesticide mixture and tested with the same CQDs solution to assess their impact on the fluorescence intensity. Gradually increasing the concentrations of the pesticide mixture from 0.2 to 5000 ng/mL led to a transformation of the original green color of the CQDs into a colorless solution under UV light. Fluorescence intensity quenching typically commenced with the rising concentration of the four selected pesticide mixtures, as depicted in Figure 7. Analysis of the correlation between pesticide concentrations and logarithmic fluorescence intensities revealed a strongly negative correlation value of −0.95. There exists a trade-off between the fluorescence intensity and pesticide concentration.

3.3. Mechanism of Fluorescence "Turn On and Off". During the experiment, it was observed that a reciprocal relationship existed between the pesticide concentration and fluorescence intensity when all four pesticides were tested. This underscores the pivotal role of CQDs in modulating fluorescence through FRET in pesticide detection, as illustrated in Figures 8 and 9. The diagram elucidates the distribution of the fluorescence energy between CQDs and pesticides. Utilizing intermolecular long-range dipole−dipole coupling, an excited molecular fluorophore (the donor) can transfer energy nonradiatively to another fluorophore (the acceptor) via a distance-dependent physical mechanism. Additionally, CQDs can alter their fluorescence intensity by self-complexation in the presence of pesticides.

3.4. Interaction between CQDs and Pesticides within a Tea Infusion. The fluorescence sensing behavior of CQDs for quinalphos 25 EC, thiamethoxam 25 WG, propargite 57 EC, and hexaconazole 5 EC within a tea infusion from the experimental sample was investigated to assess the practical applicability of this method. Processed tea leaves available on the market often contain various combinations of pesticides at differing concentrations. Thus, the quenching behavior of various pesticide mixtures (quinalphos 25 EC, thiamethoxam 25 WG, propargite 57 EC, and hexaconazole 5 EC) in experimental tea infusion samples mixed with green CQDs was recorded, as depicted in Figure 10.

The quenching intensities observed in the experimental sample of tea infusion were lower than those observed in the solution containing only CQDs with pesticides. This difference in fluorescence intensities can be ascribed to the presence of polyphenols in tea, which are known for their antioxidant properties. These polyphenols interact with the CQDs and slightly diminish the fluorescence intensities, although not entirely quenching them.

CQDs exhibited significant quenching at various concentrations (0.2, 1, 10, 50, 250, 1000, 2500, and 5000 ng/mL) of pesticide mixture. This observation was further validated by a photograph captured under UV light (Figure 10). With increasing concentrations of the pesticide mixture, the fluorescence intensity decreased. This outcome aligns with the quenching trend observed when individual pesticides interact with CQDs. Thiamethoxam 25 WG and propargite 57 EC demonstrated fluorescence quenching, while quinalphos 25 EC exhibited fluorescence-enhancing behavior. Conversely, hexaconazole 5 EC showed no significant changes in the fluorescence intensity. However, in a mixture of all of the pesticides, it was observed that the fluorescence intensity decreased with increasing concentrations of the pesticides. This phenomenon likely reflects the varying binding affinities of each pesticide, which may override each other's natural interactions and result in quenching of the CQDs' fluorescence. The four pesticides may have engaged in hydrogen bonding and ionic interactions with the surface groups of the CQDs in an aqueous environment. During this interaction, the intensity of CQDs was quenched due to the

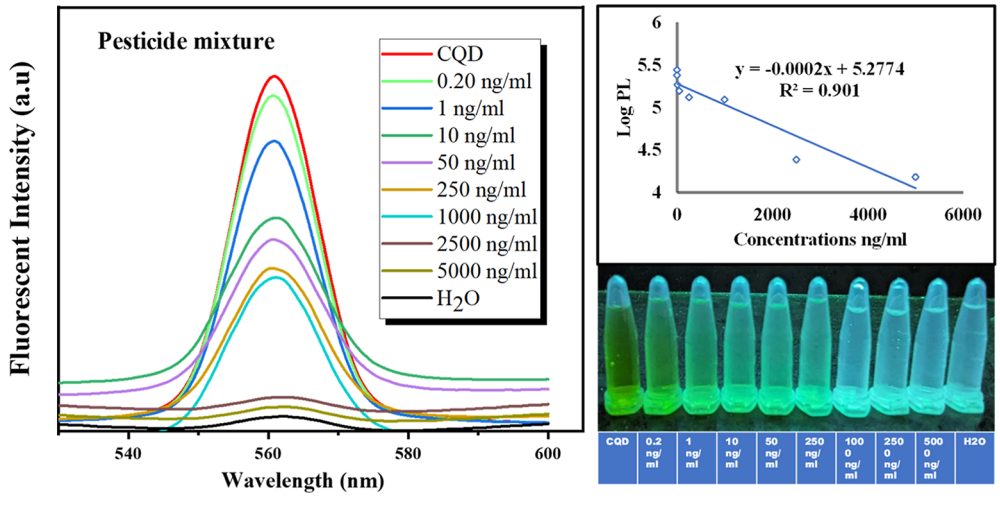

Figure 7. Pesticide mixture with CQDs and the corresponding graphical representation.

https://doi.org/10.1021/acsomega.4c04449
ACS Omega 2024, 9, 50201−50213

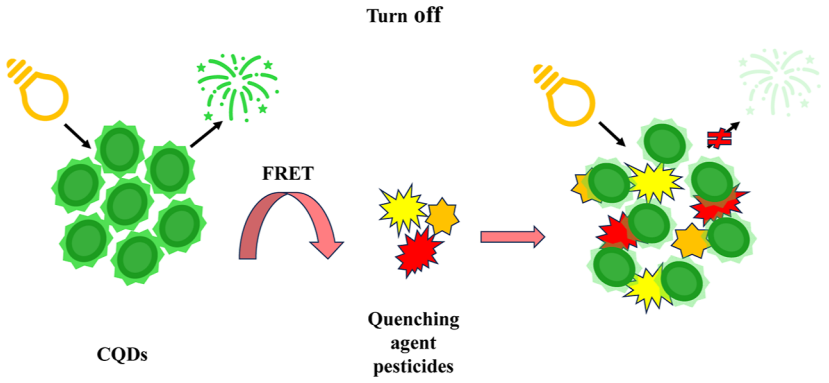

Figure 8. "Turn off" mechanism of fluorescence intensity due to the addition of fluorescence quenching pesticides.

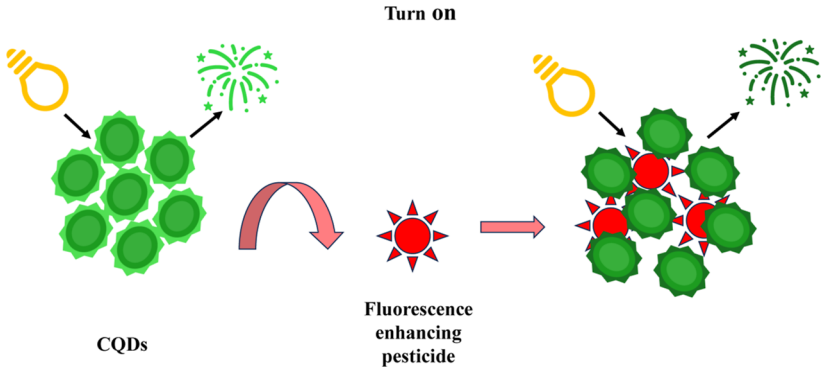

Figure 9. Fluorescence intensity "turn on" mechanism triggered by the inclusion of a fluorescence-enhancing pesticide.

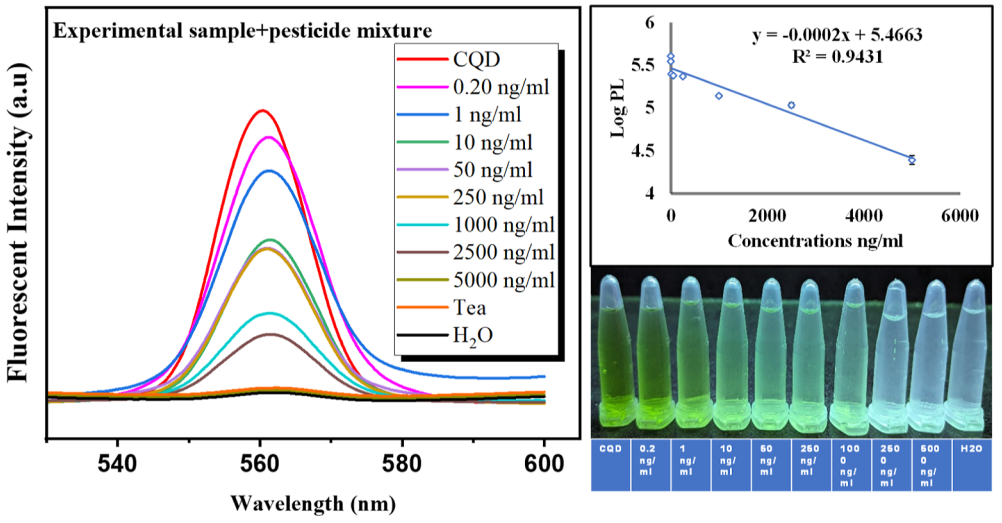

Figure 10. Effects of pesticide mixture on the experimental sample and the corresponding linear graphical representation.

high binding affinity and selectivity toward thiamethoxam 25 WG and propargite 57 EC. The fluorescence intensity was quenched, presumably due to energy transfer between the CQDs and pesticides following the FRET mechanism.

Following this, we assessed the linear relationship between pesticide concentrations and logarithmic fluorescence intensities (depicted in Figure 10) to rigorously validate the sensitivity of the reaction. The pesticide mixture exhibited a robust negative correlation value of −0.97, indicating that as pesticide concentrations increase, the fluorescence intensity decreases. In summary, the specificity of the synthesized CQDs is affirmed by their lack of fluorescence quenching when interacting with hexaconazole 5 EC. The estimated detection limits for quinalphos 25 EC, thiamethoxam 25 WG, and propargite 57 EC are 0.2, 1, and 10 ng/mL, respectively. This study boasts the lowest detection limit compared with widely employed detection methodologies in previous research, encompassing chromatography, carbon dots detection, and various forms of CE. The synthesized CQDs demonstrate the capability to detect quinalphos 25 EC, thiamethoxam 25 WG, propargite 57 EC, and hexaconazole 5 EC in experimental samples. Moreover, owing to their effective quenching properties, the simultaneous detection of all four pesticides in a single sample is also achievable.

https://doi.org/10.1021/acsomega.4c04449
ACS Omega 2024, 9, 50201−50213

4. CONCLUSIONS

CQDs synthesized from tea waste exhibited a remarkable quantum yield of 40.05%. The fluorescence of CQDs was modulated by quinalphos 25 EC, thiamethoxam 25 WG, and propargite 57 EC, both individually and in combination with hexaconazole 5 EC, showcasing efficient fluorescence quenching. Our study reported detection limits ranging from 0.2 to 10 ng/mL. The synthesized CQDs demonstrated high stability and facilitated rapid pesticide detection. Moreover, our findings revealed the capability of detecting four pesticides simultaneously in a single sample, owing to their effective quenching properties. Thus, our research offers valuable insights into the practical application of CQDs derived from waste tea leaves (post tea infusion preparation) for the specific, swift, and low-level detection of pesticides in processed tea leaves.

AUTHOR INFORMATION

Corresponding Author

Sonali Ray − *Tea Chemistry and Pharmacology Laboratory, Department of Tea Science, University of North Bengal, Siliguri, West Bengal 734013, India;* orcid.org/0000-0002-3742-8356; Email: sonaliray@nbu.ac.in

Author

Nitu Sinha − *Tea Chemistry and Pharmacology Laboratory, Department of Tea Science, University of North Bengal, Siliguri, West Bengal 734013, India*

Complete contact information is available at: https://pubs.acs.org/10.1021/acsomega.4c04449

Author Contributions

During all phases of experimentation, Nitu Sinha conducted sample collection, preparation, and biochemical analysis as well as drafted the article. Dr. Sonali Ray conceptualized and designed the research project and contributed to drafting the manuscript. All authors critically reviewed and approved the final version of the manuscript.

Notes

The authors declare no competing financial interest.

ACKNOWLEDGMENTS

The authors acknowledge the financial support from the Swami Vivekananda merit-cum-means (SVMCM) fellowship, utilized by the first author, and the North Bengal University Research Grant. They also extend gratitude to the Sophisticated Analysis Instrumentation Facility (SAIF) at AIIMS New Delhi for facilitating HRTEM characterization. Special thanks are due to Prof. Kanishka Biswas and the SAMat Research Facilities, JNCSAR, Bengaluru, for their assistance with XPS characterization. The authors express appreciation to Prof. Pranab Ghosh, Debosmita Mukherjee, and Munna Mukhia from the Department of Chemistry at the University of North Bengal for their guidance during PL and Raman spectroscopy experimentation. Additionally, the authors are thankful to Dr. Kalyan Jyoti Sarkar from the Department of Inorganic Chemistry at the University of Chemistry and Technology, Prague, for his support with XRD and AFM analysis.

REFERENCES

(1) Shrestha, G.; Thapa, R. B. Tea Pests and Pesticide Problems and Integrated Management. *J. Agric. Environ.* **2015**, *16*, 188−200.

(2) Liang, N.; Hu, X.; Li, W.; Mwakosya, A. W.; Guo, Z.; Xu, Y.; Huang, X.; Li, Z.; Zhang, X.; Zou, X.; Shi, J. Fluorescence and Colorimetric Dual-Mode Sensor for Visual Detection of Malathion in Cabbage Based on Carbon Quantum Dots and Gold Nanoparticles. *Food Chem.* **2021**, *343*, 128494.

(3) Hazarika, L. K.; Bhuyan, M.; Hazarika, B. N. Insect Pests of Tea and Their Management. *Annu. Rev. Entomol.* **2009**, *54*, 267−284.

(4) Xu, W.; Hao, X.; Li, T.; Dai, S.; Fang, Z. Dual-Mode Fluorescence and Visual Fluorescent Test Paper Detection of Copper Ions and EDTA. *ACS Omega* **2021**, *6* (43), 29157−29165.

(5) Hou, R. Y.; Jiao, W. T.; Qian, X. S.; Wang, X. H.; Xiao, Y.; Wan, X. C. Effective Extraction Method for Determination of Neonicotinoid Residues in Tea. *J. Agric. Food Chem.* **2013**, *61* (51), 12565−12571.

(6) Llorent-Martínez, E. J.; Soler-Gallardo, M. I.; Ruiz-Medina, A. Determination of Thiacloprid, Thiamethoxam and Imidacloprid in Tea Samples by Quenching Terbium Luminescence. *Luminescence* **2019**, *34* (5), 460−464.

(7) Dong, X.; Zhu, B.; Zhao, X.; Wang, H.; Liu, S. Transfer Rates on Nine Pesticides from Dry Tea to Infusion by QuEChERS Purification Followed by LC-MS/MS Analysis. *Int. J. Environ. Anal. Chem.* **2023**, *103* (13), 2931−2947.

(8) Li, X.; Zhang, Z.; Li, P.; Zhang, Q.; Zhang, W.; Ding, X. Determination for Major Chemical Contaminants in Tea (*Camellia sinensis*) Matrices: A Review. *Food Res. Int.* **2013**, *53* (2), 649−658.

(9) Timchenko, Y. V. Advantages and Disadvantages of High-Performance Liquid Chromatography (HPCL). *J. Environ. Anal. Chem.* **2021**, *8* (10), 335.

(10) Jornet-Martínez, N.; Moliner-Martínez, Y.; Molins-Legua, C.; Campíns-Falcó, P. Trends for the Development of In Situ Analysis Devices. In *Encyclopedia of Analytical Chemistry*; Wiley, 2017; pp 1−23.

(11) Gummadi, S.; Kandula, V. N. A review on electrophoresis, capillary electrophoresis and hyphenations. *Int. J. Pharm. Sci. Res.* **2020**, *11* (12), 6038.

(12) Gupta, M. K.; Ghuge, A.; Parab, M.; Al-Refaei, Y.; Khandare, A.; Dand, N.; Waghmare, N. A Comparative Review on High-Performance Liquid Chromatography (HPLC), Ultra Performance Liquid Chromatography (UPLC) & High-Performance Thin Layer Chromatography (HPTLC) with Current Updates. *Curr. Issues Pharm. Med. Sci.* **2022**, *35* (4), 224−228.

(13) Liu, X.; Cheng, H.; Zhao, Y.; Wang, Y.; Li, F. Portable Electrochemical Biosensor Based on Laser-Induced Graphene and MnO2 Switch-Bridged DNA Signal Amplification for Sensitive Detection of Pesticide. *Biosens. Bioelectron.* **2022**, *199*, 113906.

(14) Gai, P.; Pu, L.; Wang, C.; Zhu, D.; Li, F. CeO2@NC Nanozyme with Robust Dephosphorylation Ability of Phosphotriester: A Simple Colorimetric Assay for Rapid and Selective Detection of Paraoxon. *Biosens. Bioelectron.* **2023**, *220*, 114841.

(15) Zhu, D.; Zhang, M.; Pu, L.; Gai, P.; Li, F. Nitrogen-Enriched Conjugated Polymer Enabled Metal-Free Carbon Nanozymes with Efficient Oxidase-Like Activity. *Small* **2022**, *18* (3), 2104993.

(16) Chang, J.; Yu, L.; Hou, T.; Hu, R.; Li, F. Direct and Specific Detection of Glyphosate Using a Phosphatase-like Nanozyme-Mediated Chemiluminescence Strategy. *Anal. Chem.* **2023**, *95* (9), 4479−4485.

(17) Yu, L.; Chang, J.; Zhuang, X.; Li, H.; Hou, T.; Li, F. Two-Dimensional Cobalt-Doped Ti3C2MXene Nanozyme-Mediated Homogeneous Electrochemical Strategy for Pesticides Assay Based on In Situ Generation of Electroactive Substances. *Anal. Chem.* **2022**, *94* (8), 3669−3676.

(18) Berhanu, S.; Habtamu, F.; Tadesse, Y.; Gonfa, F.; Tadesse, T. Fluorescence Sensor Based on Polyaniline Supported Ag-ZnO Nanocomposite for Malathion Detection. *J. Sens.* **2022**, *2022* (1), 1−11.

https://doi.org/10.1021/acsomega.4c04449
ACS Omega 2024, 9, 50201−50213

(19) Liu, B.; Chen, J.; Peng, Y.; Xiao, W.; Peng, Z.; Qiu, P. Graphitic-Phase C3N4 Nanosheets Combined with MnO2 Nanosheets for Sensitive Fluorescence Quenching Detection of Organophosphorus Pesticides. *J. Environ. Sci. Health, Part B* **2022**, *57* (6), 441−449.
(20) Gaviria, M. I.; Barrientos, K.; Arango, J. P.; Cano, J. B.; Peñuela, G. A. Highly Sensitive Fluorescent Biosensor Based on Acetylcholinesterase and Carbon Dots−Graphene Oxide Quenching Test for Analytical and Commercial Organophosphate Pesticide Detection. *Front. Environ. Sci.* **2022**, *10*, 825112.
(21) Tseng, W. B.; Hsieh, M. M.; Chen, C. H.; Chiu, T. C.; Tseng, W. L. Functionalized Gold Nanoparticles for Sensing of Pesticides: A Review. *J. Food Drug Anal.* **2020**, *28* (4), 522−539.
(22) Goel, P.; Arora, M. Fabrication of Chemical Sensor for Organochlorine Pesticide Detection Using Colloidal Gold Nanoparticles. *MRS Commun.* **2018**, *8* (3), 1000−1007.
(23) Jin, Y.; Liu, K.; Li, G.; Li, C.; Xiao, Z.; Yuan, C.; Li, J. In Situ Reduction Triggers the Highly Sensitive Detection of Pesticide by Classic Gold Nanoparticle and Quantum Dots Nanocomposite. *Anal. Chim. Acta* **2021**, *1172*, 338679.
(24) Cheng, N.; Song, Y.; Fu, Q.; Du, D.; Luo, Y.; Wang, Y.; Xu, W.; Lin, Y. Aptasensor Based on Fluorophore-Quencher Nano-Pair and Smartphone Spectrum Reader for on-Site Quantification of Multi-Pesticides. *Biosens. Bioelectron.* **2018**, *117*, 75−83.
(25) Zuo, P.; Lu, X.; Sun, Z.; Guo, Y.; He, H. A Review on Syntheses, Properties, Characterization and Bioanalytical Applications of Fluorescent Carbon Dots. *Microchim. Acta* **2016**, *183*, 519−542.
(26) Romero, V.; Vila, V.; de la Calle, I.; Lavilla, I.; Bendicho, C. Turn−on Fluorescent Sensor for the Detection of Periodate Anion Following Photochemical Synthesis of Nitrogen and Sulphur Co−Doped Carbon Dots from Vegetables. *Sens. Actuators, B* **2019**, *280*, 290−297.
(27) Alam, A. M.; Park, B. Y.; Ghouri, Z. K.; Park, M.; Kim, H. Y. Synthesis of Carbon Quantum Dots from Cabbage with Down- and up-Conversion Photoluminescence Properties: Excellent Imaging Agent for Biomedical Applications. *Green Chem.* **2015**, *17* (7), 3791−3797.
(28) Vibhute, A.; Patil, T.; Gambhir, R.; Tiwari, A. P. Fluorescent Carbon Quantum Dots: Synthesis Methods, Functionalization and Biomedical Applications. *Appl. Surface Sci. Adv.* **2022**, *11*, 100311.
(29) Rocco, D.; Moldoveanu, V. G.; Feroci, M.; Bortolami, M.; Vetica, F. Electrochemical Synthesis of Carbon Quantum Dots. *Chemelectrochem* **2023**, *10* (3), No. e202201104.
(30) Dubey, P.; Nimbalkar, T.; Sahu, V.; Bano, S. A Review on Synthesis and Application of Carbon Quantum Dots. *Eur. Chem. Bull.* **2023**, *12* (5), 1509−1518.
(31) Yilmaz, T. The Hydrothermal Synthesis of Blue-Emitting Boron-Doped CQDs and Its Application for Improving the Photovoltaic Parameters of Organic Solar Cell. *Turk. J. Chem.* **2021**, *45* (6), 1828−1840.
(32) Kumar, A.; Kumar, I.; Gathania, A. K. Synthesis, Characterization and Potential Sensing Application of Carbon Dots Synthesized via the Hydrothermal Treatment of Cow Milk. *Sci. Rep.* **2022**, *12* (1), 22495.
(33) Atchudan, R.; Edison, T. N. J. I.; Shanmugam, M.; Perumal, S.; Somanathan, T.; Lee, Y. R. Sustainable Synthesis of Carbon Quantum Dots from Banana Peel Waste Using Hydrothermal Process for in Vivo Bioimaging. *Phys. E* **2021**, *126*, 114417.
(34) He, M.; Zhang, J.; Wang, H.; Kong, Y.; Xiao, Y.; Xu, W. Material and Optical Properties of Fluorescent Carbon Quantum Dots Fabricated from Lemon Juice via Hydrothermal Reaction. *Nanoscale Res. Lett.* **2018**, *13*, 1−7.
(35) Khor, Y.; Abdul Aziz, A. R.; Chong, S. S. Synthesis of Carbon-Based Quantum Dots Using Lemon Juice under Hydrothermal Method. *Int. J. Nanoelectron. Mater.* **2022**, *15*, 241.
(36) Qu, J. H.; Wei, Q.; Sun, D. W. Carbon Dots: Principles and Their Applications in Food Quality and Safety Detection. *Crit. Rev. Food Sci. Nutr.* **2018**, *58* (14), 2466−2475.
(37) Wu, J.; Chen, X.; Zhang, Z.; Zhang, J. Off-on" Fluorescence Probe Based on Green Emissive Carbon Dots for the Determination of Cu2+ Ions and Glyphosate and Development of a Smart Sensing Film for Vegetable Packaging. *Microchim. Acta* **2022**, *189* (3), 131.
(38) Zhang, R.; Zhang, L.; Yu, R.; Wang, C. Rapid and Sensitive Detection of Methyl Parathion in Rice Based on Carbon Quantum Dots Nano-Fluorescence Probe and Inner Filter Effect. *Food Chem.* **2023**, *413*, 135679.
(39) Yang, Y.; Huo, D.; Wu, H.; Wang, X.; Yang, J.; Bian, M.; Ma, Y.; Hou, C. N. P-Doped Carbon Quantum Dots as a Fluorescent Sensing Platform for Carbendazim Detection Based on Fluorescence Resonance Energy Transfer. *Sens. Actuators, B* **2018**, *274*, 296−303.
(40) Li, H.; Deng, R.; Tavakoli, H.; Li, X.; Li, X. J. Ultrasensitive Detection of Acephate Based on Carbon Quantum Dot-Mediated Fluorescence Inner Filter Effects. *Analyst* **2022**, *147* (23), 5462−5469.
(41) Xu, W.; Hao, X.; Li, T.; Dai, S.; Fang, Z. Dual-Mode Fluorescence and Visual Fluorescent Test Paper Detection of Copper Ions and EDTA. *ACS Omega* **2021**, *6* (43), 29157−29165.
(42) Zhang, H.; Hao, X.; Xu, Y.; Wang, S.; Dai, S.; Xu, W. Preparation of Fluorescent Materials from Soybean Pods and Their Applications in Environmental Monitoring and Pharmaceutical Analysis. *J. Mater. Sci.: Mater. Electron.* **2022**, 33 (25), 19910−19922.
(43) Zhu, J.; Zhu, F.; Yue, X.; Chen, P.; Sun, Y.; Zhang, L.; Mu, D.; Ke, F. Waste Utilization of Synthetic Carbon Quantum Dots Based on Tea and Peanut Shell. *J. Nanomater.* **2019**, *2019* (1), 1−7.
(44) Liu, Y.; Liu, Y.; Park, M.; Park, S. J.; Zhang, Y.; Akanda, M. R.; Park, B. Y.; Kim, H. Y. Green Synthesis of Fluorescent Carbon Dots from Carrot Juice for in Vitro Cellular Imaging. *Carbon Lett.* **2017**, *21* (1), 61−67.
(45) Chunduri, L. A. A.; Kurdekar, A.; Patnaik, S.; Dev, B. V.; Rattan, T. M.; Kamisetti, V. Carbon Quantum Dots from Coconut Husk: Evaluation for Antioxidant and Cytotoxic Activity. *Mater. Focus* **2016**, *5* (1), 55−61.
(46) Mondal, T. K.; Ghorai, U. K.; Saha, S. K. Dual-Emissive Carbon Quantum Dot-Tb Nanocomposite as a Fluorescent Indicator for a Highly Selective Visual Detection of Hg(II) in Water. *ACS Omega* **2018**, *3* (9), 11439−11446.
(47) Chen, K.; Qing, W.; Hu, W.; Lu, M.; Wang, Y.; Liu, X. On-off-on Fluorescent Carbon Dots from Waste Tea: Their Properties, Antioxidant and Selective Detection of CrO 42−, Fe 3+, Ascorbic Acid and L-Cysteine in Real Samples. *Spectrochim. Acta, Part A* **2019**, *213*, 228−234.
(48) Wei, J.; Liu, B.; Yin, P. Dual Functional Carbonaceous Nanodots Exist in a Cup of Tea. *RSC Adv.* **2014**, *4* (108), 63414−63419.
(49) Li, R.; Zhu, Z.; Pan, P.; Liu, J.; Zhou, B.; Liu, C.; Yang, Z.; Wang, J.; Li, X.; Yang, X.; Chang, J.; Niu, H. One-Step Synthesis of Nitrogen-Doped Carbon Quantum Dots for Paper-Based Electrochemiluminescence Detection of Cu2+ Ions. *Microchem. J.* **2022**, *174*, 107057.
(50) Mehta, V. N.; Jha, S.; Basu, H.; Singhal, R. K.; Kailasa, S. K. One-Step Hydrothermal Approach to Fabricate Carbon Dots from Apple Juice for Imaging of Mycobacterium and Fungal Cells. *Sens. Actuators, B* **2015**, *213*, 434−443.
(51) Qin, X.; Lu, W.; Asiri, A. M.; Al-Youbi, A. O.; Sun, X. Green, Low-Cost Synthesis of Photoluminescent Carbon Dots by Hydrothermal Treatment of Willow Bark and Their Application as an Effective Photocatalyst for Fabricating Au Nanoparticles-Reduced Graphene Oxide Nanocomposites for Glucose Detection. *Catal. Sci. Technol.* **2013**, 3 (4), 1027−1035.
(52) Xu, Y.; Tang, C. J.; Huang, H.; Sun, C. Q.; Zhang, Y. K.; Ye, Q. F.; Wang, A. J. Green Synthesis of Fluorescent Carbon Quantum Dots for Detection of Hg2+. *Chin. J. Anal. Chem.* **2014**, *42* (9), 1252−1258.
(53) Yang, K.; Liu, M.; Wang, Y.; Wang, S.; Miao, H.; Yang, L.; Yang, X. Carbon Dots Derived from Fungus for Sensing Hyaluronic Acid and Hyaluronidase. *Sens. Actuators, B* **2017**, *251*, 503−508.
(54) Huang, H.; Lv, J. J.; Zhou, D. L.; Bao, N.; Xu, Y.; Wang, A. J.; Feng, J. J. One-Pot Green Synthesis of Nitrogen-Doped Carbon

https://doi.org/10.1021/acsomega.4c04449
ACS Omega 2024, 9, 50201−50213

Nanoparticles as Fluorescent Probes for Mercury Ions. *RSC Adv.* **2013**, *3* (44), 21691−21696.
(55) Liu, Y.; Liu, Y.; Park, M.; Park, S. J.; Zhang, Y.; Akanda, M. R.; Park, B. Y.; Kim, H. Y. Green Synthesis of Fluorescent Carbon Dots from Carrot Juice for in Vitro Cellular Imaging. *Carbon Lett.* **2017**, *21* (1), 61−67.
(56) Sahu, S.; Behera, B.; Maiti, T. K.; Mohapatra, S. Simple One-Step Synthesis of Highly Luminescent Carbon Dots from Orange Juice: Application as Excellent Bio-Imaging Agents. *Chem. Commun.* **2012**, *48* (70), 8835−8837.
(57) Aparajita, N.; Chandan, R. S.; Tengli, A. K.; Mohan, S. P.; Tejas, T. S.; Kavyashree, R.; Moksha, C.; Sujan, K. M.; Sinchana, M. A.; Yashaswini, R. Analytical Method Development And Validation Of Thiamethoxam By Rp-Hplc Method. *J. Pharm. Negat. Results* **2022**, *13* (7), 1682−1692.
(58) Ganesamurthi, J.; Keerthi, M.; Chen, S. M.; Shanmugam, R. Electrochemical Detection of Thiamethoxam in Food Samples Based on Co3O4 Nanoparticle@Graphitic Carbon Nitride Composite. *Ecotoxicol. Environ. Saf.* **2020**, *189*, 110035.
(59) Yue, Y.; Zhang, D.; Tian, K.; Ni, D.; Guo, F.; Yu, Z.; Wang, P.; Liang, P. Screening and Evaluation of Thiamethoxam Aptamer Based on Pressurized GO-SELEX and Its Sensor Application. *Biosensors* **2023**, *13* (2), 155.
(60) Hu, H.; Liu, X.; Jiang, F.; Yao, X.; Cui, X. A Novel Chemiluminescence Assay of Organophosphorous Pesticide Quinalphos Residue in Vegetable with Luminol Detection. *Chem. Cent J.* **2010**, *4* (1), 1−6.
(61) Neog, K.; Dhanakodi, K.; Muraleedharan, N. N. Residues of Propargite in Tea. *Int. J. Agric Sci. Food Technol.* **2015**, *1* (1), 012−015.
(62) Patil, V. K.; Dhande, N. D.; Petha, N. H.; Narkhede, H. P. A. Simple Derivatization RP-HPLC Method for the Simultaneous Determination of Zineb and Hexaconazole in Pesticide Formulation Using a PDA Detector. *Anal. Methods* **2021**, *13* (35), 3930−3939.

https://doi.org/10.1021/acsomega.4c04449
ACS Omega 2024, 9, 50201−50213